ACS OMEGA

Article

Cite This: ACS Omega 2018, 3, 11151−11162

http://pubs.acs.org/journal/acsodf

Bispyranopyrazoles as Green Corrosion Inhibitors for Mild Steel in Hydrochloric Acid: Experimental and Theoretical Approach

Priyanka Singh,*[,†] Madhan Kumar,[§] Mumtaz Ahmad Quraishi,*[,§] Jiyaul Haque,[‡] and Gurmeet Singh[†]

[†]Department of Chemistry, University of Delhi, Delhi 110007, India

[‡]Department of Chemistry, Indian Institute of Technology (Banaras Hindu University), Varanasi 221005, India

[§]Center of Research Excellence in Corrosion, Research Institute, King Fahd University of Petroleum & Minerals, Dhahran 31261, Saudi Arabia

ABSTRACT: In the present study, we have synthesized two novel corrosion inhibitors BP-1 and BP-2 and evaluated their corrosion inhibition property on mild steel (MS) in acid solution through weight loss and electrochemical corrosion techniques. The corrosion test results reveal that both compounds inhibit corrosion by an adsorption mechanism and display inhibition efficiency more than 95% at a low concentration of 1.72×10^{-4} M. From the surface analysis of the protective film on MS, it was corroborated that adsorption of inhibitor molecules occurred on the MS surface through chemisorption, which further suppresses the corrosion rate. Density functional theory simulated data helps correlate the experimental trend with the theoretical study.

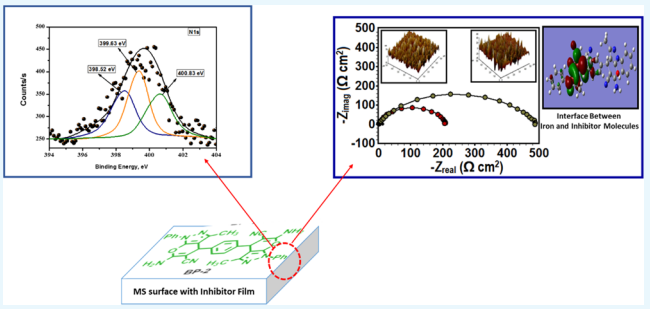

1. INTRODUCTION

Pyranopyrazoles have been considered as a significant category of heterocyclic compounds due to their widespread applications in pharmaceuticals and biodegradable agrochemicals.[1] Pyranopyrazole compounds exhibited numerous biological activities like anticancer, antibacterial, antiherpetic, and molluscicidal activities.[2] These observations have prompted us to evaluate corrosion inhibition characteristics of bispyranopyrazoles (BPs). BPs have been selected in the present investigation as corrosion inhibitors because they are highly functionalized heterocyclic compounds with NH_2 and CN as functional groups and possess four N and two O atoms in the ring, besides π electrons, through which they can readily attach on the surface of mild steel (MS) and bring down the corrosion rate.[3] Another interesting feature is that they can be synthesized very easily by multicomponent one-pot reactions with good yields using green chemistry principles.[2]

In the present investigation, we have used a theoretical method, density functional theory (DFT), to perceive the corrosion inhibition efficiency (IE) of the studied compounds. These techniques are inexpensive and time-saving, provide detailed information about the mechanism of corrosion inhibition in comparison with traditional methods, and help simulate the obtained experimental results with estimated molecular properties (high occupied molecular orbital energy) (E_{HOMO}), low unoccupied molecular energy (E_{LUMO}), energy gap (ΔE), global softness (GS, σ), global hardness (GH, η), electronegativity (χ), and fraction of electrons transferred (ΔN) from BPs to MS.[4−6]

Our research group has reported earlier four pyranopyrazoles that showed corrosion inhibition efficiency (88−98%) at 200 mg/L.[7] In the present effort, we have synthesized two new corrosion inhibitors BP-1 and BP-2, which are likely to give enhanced inhibition efficiency compared to that of earlier reported pyranopyrazoles at lower concentrations because these molecules are more functionalized than previously reported pyrazoles. We have compared the inhibition performance of BPs with some previously reported inhibitors and found their better corrosion inhibition performance. Gupta et al. have reported α-aminophosphonates as corrosion inhibitors for mild steel. These inhibitors gave 58−96% IE at (141−564) $\times 10^{-6}$ M. Wang et al. reported *S*-benzyl-*O*,*O*′-bis(2-naphthyl)dithiophosphates as corrosion inhibitors, which showed IE of 70−95% at 40−100 mg/L.[8,9] To the best of our knowledge, there is no previous investigation on the use of bispyranopyrazoles for the corrosion inhibition of metallic substrates in an acidic environment.

Herein, we investigate the application of two interface inhibitors BP-1 and BP-2 for the corrosion inhibition of MS samples in an acidic environment through gravimetric and electrochemical measurements. Surface characterizations of MS samples without and with BPs were performed to analyze the protective inhibitor film. Quantum chemical theoretical studies were also performed to investigate the correlations between experimental observations and the quantum chemically calculated values (Table 1).

Received: June 11, 2018
Accepted: August 31, 2018
Published: September 14, 2018

DOI: 10.1021/acsomega.8b01300
ACS Omega 2018, 3, 11151−11162

Table 1. Molecular Structures of Bispyrano[2,3-*c*]pyrazoles

Inhibitors	Molecular Structures
4,4'-(1,4-phenylene)bis(6-amino-3-methyl-2,4-dihydropyrano[2,3-c]pyrazole-5-carbonitrile) (BP-1)	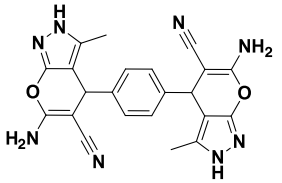
4,4'-(1,4-phenylene)bis(6-amino-3-methyl-1-phenyl-1,4-dihydropyrano[2,3-c]pyrazole-5-carbonitrile) (BP-2)	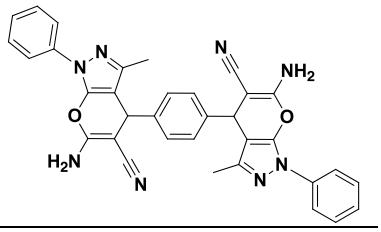

2. RESULTS AND DISCUSSION

2.1. Gravimetric Measurements. The gravimetric measurement results for MS samples in test acidic solution in the presence and absence of BPs are summarized in Table 2.

Table 2. Gravimetric Measurements for MS in the Absence and Presence of Bispyrano[2,3-*c*]pyrazoles in 1 M HCl at 308 K

inhibitors	conc. (mol)	corrosion rate ($mg/cm^2/h$)	surface coverage (θ)	η%
blank	0.0	5.03		
BP-1	4.31×10^{-5}	0.70	0.85	85.09 (2.3)
	8.63×10^{-5}	0.40	0.92	92.05 (1.4)
	1.29×10^{-4}	0.26	0.94	94.70 (1.8)
	1.72×10^{-4}	0.20	0.96	96.02 (0.8)
BP-2	4.31×10^{-5}	0.53	0.89	89.40 (1.45)
	8.63×10^{-5}	0.25	0.95	95.03 (1.63)
	1.29×10^{-4}	0.15	0.97	97.01 (1.48)
	1.72×10^{-4}	0.10	0.98	98.01 (1.26)

It is a reliable approach to optimize the influence of concentrations of the corrosion inhibitor on inhibition effectiveness (Figure 1).[10] The obtained results indicated that addition of BP-1 and BP-2 prevents the MS against corrosion and also the corrosion inhibition efficiency increases with the increase in concentration of BPs, presented in Figure 2. Of the two inhibitors, BP-2 shows higher inhibition

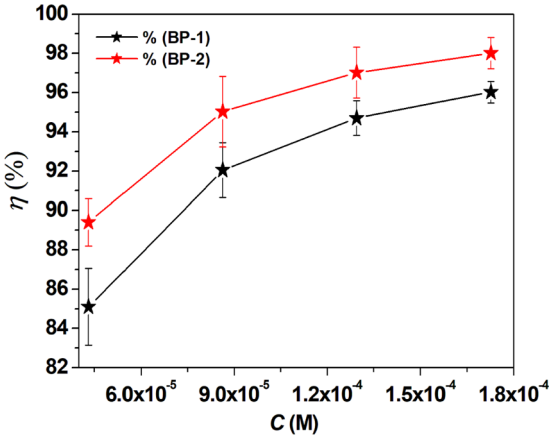

Figure 2. Effect of different concentrations of bispyrano[2,3-*c*]pyrazoles on the inhibition efficiency for MS in 1 M HCl.

efficiency, and the order of inhibition is BP-2 (98.01%) > BP-1 (96.02%) at 1.72×10^{-4} M. Furthermore, the good inhibition performance is ascribed to the attachment of BP molecules on the MS surface, which is supported due to the existence of numerous heteroatoms (N, O) in BPs with large molecular structure of BPs. Furthermore, the variance in the corrosion inhibition efficiency between BP-1 and BP-2 is ascribed to the nature of the substituent group attached to the pyrazole ring. In the BP-2 molecule, the presence of phenyl group increases the electron density at the active centers, which facilitates more interaction of this inhibitor with the MS steel surface as compared to that of BP-1, which is devoid of substituents.[11]

2.1.1. Adsorption Isotherms. The obtained values of surface coverage (θ) by gravimetric measurements for BP-1 and BP-2 were used to find the best-fitted adsorption isotherms. The adsorption isotherms help understand the interaction between the inhibitor molecules and the metal surface. The inhibitor molecules adsorb on the metal surface either physically or chemically. To understand the adsorption phenomenon, different adsorption isotherms (Temkin, Freundlich, and

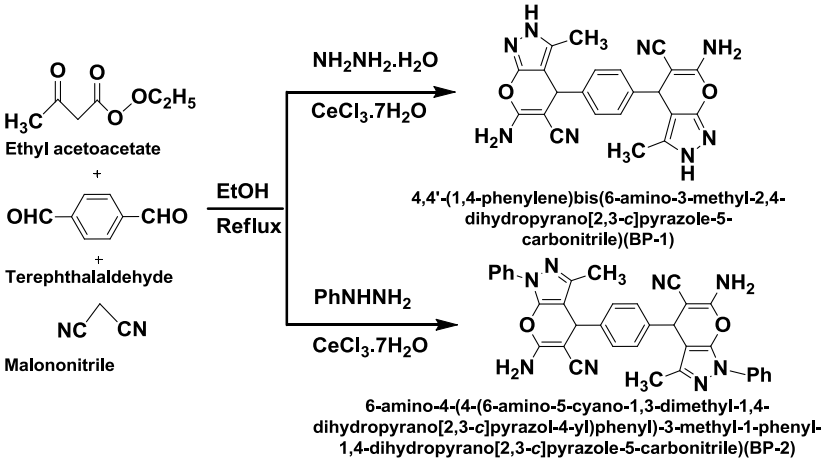

Figure 1. Synthetic route for the preparation of bispyrano[2,3-*c*]pyrazoles.

DOI: 10.1021/acsomega.8b01300
ACS Omega 2018, 3, 11151−11162

Langmuir isotherms) were applied to the experimental results. It was observed that the Langmuir adsorption isotherms fitted very well, with the regression coefficient (R^2) value for BP-1 and BP-2 of 1, suggesting good fitting. The obtained slope and intercept values for the Langmuir isotherm are 0.99646, 7.77607×10^{-6} for BP-1 and 0.98767, 5.62968×10^{-6} for BP-2. For Freundlich R^2, the slope and intercept for BP-1 are 0.95898, 0.08934, and 0.32206 and for BP-2, 0.9537, 0.06734, and 0.24743; for Temkin R^2, the slope and intercept for BP-1 are 0.95665, 0.1858, and 1.6662 and for BP-2, 0.9590, 0.1451, and 1.5318, respectively. The Langmuir adsorption isotherm

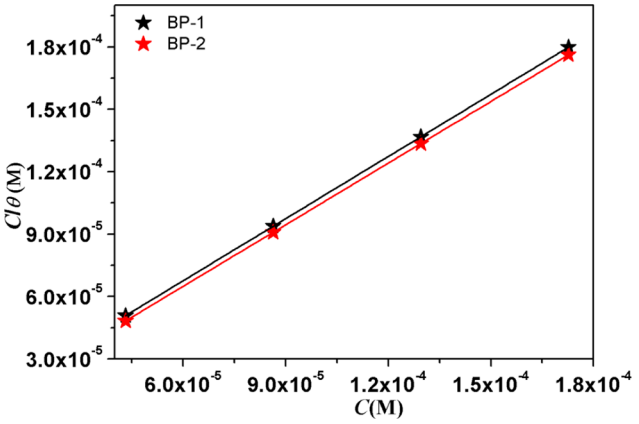

Figure 3. Langmuir adsorption isotherms for MS in the presence of bispyrano[2,3-*c*]pyrazoles.

plot between C/θ and C_i shown in Figure 3, and the equation is represented below

$$\frac{C}{\theta} = \frac{1}{K_{ads}} + C \quad (1)$$

where C represents the concentration of the inhibitor, θ is the surface area, and K_{ads} is the adsorption equilibrium constant. The K_{ads} values were obtained by a linear straight fitted plot between C/θ and C to obtain free energy of adsorption ΔG_{ads}. K_{ads} is related to ΔG_{ads} by the following equation

$$\Delta G_{ads} = -RT \ln(55.5K_{ads}) \quad (2)$$

where R is the gas constant and T is the absolute temperature. The value 55.5 is the concentration of water in solution in mol/L. By putting K_{ads} in the above equation, the ΔG_{ads} values were obtained.

It is reported that the values of ΔG_{ads} varying between −40 kJ/mol and more negative values suggest that the adsorption is chemisorption, whereas the value of ΔG_{ads} around −20 kJ/mol or less negative implies that the adsorption is due to electrostatic interaction, i.e., physisorption.[12,13] The ΔG_{ads} values for BP-1 and BP-2, i.e., 40.42 and 41.24 kJ/mol, suggest chemisorption type of adsorption.

2.2. Electrochemical Corrosion Studies. The variation obtained in open circuit potential (OCP) for MS corresponding to the reference electrode in the absence and presence of BP-1 and BP-2 is graphically represented in Figure 4. It is apparent from the OCP vs time plot that the presence of BPs shifts the steady state potential toward more negative values without changing common features. This shift in the steady state potential toward a nobler direction is attributed to

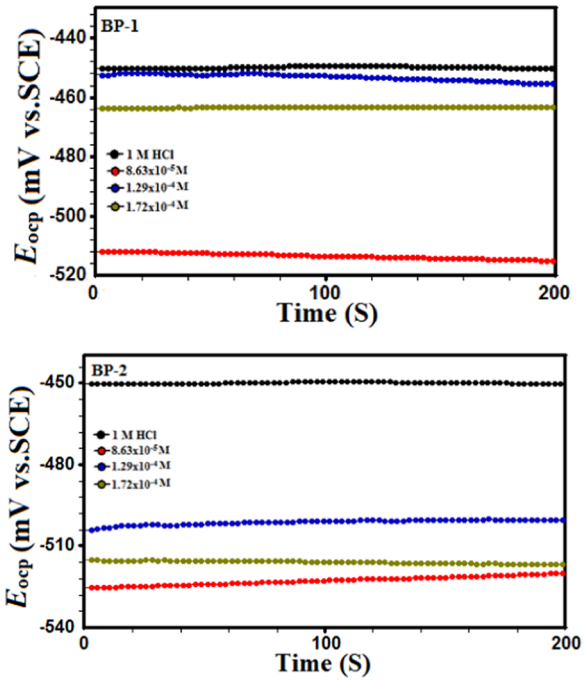

Figure 4. OCP vs time plots for MS in 1 M HCl without and with bispyrano[2,3-*c*]pyrazoles.

dissolution of the surface oxide layer and formation of a protective film of the inhibitor on the MS surface.[14]

The electrochemical impedance spectroscopy (EIS) results were analyzed with the proposed equivalent circuit diagram for MS immersed in the test solution in the presence and absence of BPs are displayed in Figures 5−7. The parameters obtained by fitted Nyquist arcs are summarized in Table 3. The equivalent circuit diagram consists of R_s (electrolytic resistance), polarization resistance (R_p), that is analogous to the constant phase element (CPE). From the Nyquist plots, it is clearly observed that both BPs exhibit one capacitive arc/loop for MS and that the diameter of the capacitive arc with

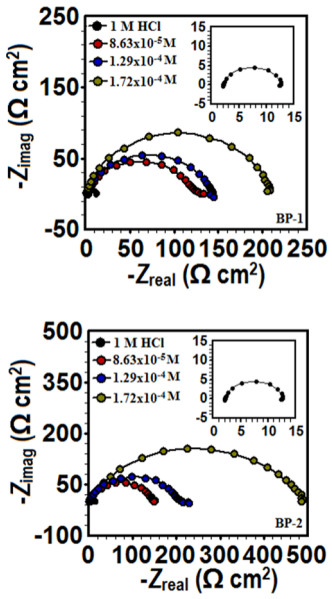

Figure 5. Nyquist plots for MS in 1 M HCl without and with bispyrano [2,3-*c*]pyrazoles.

DOI: 10.1021/acsomega.8b01300
ACS Omega 2018, 3, 11151−11162

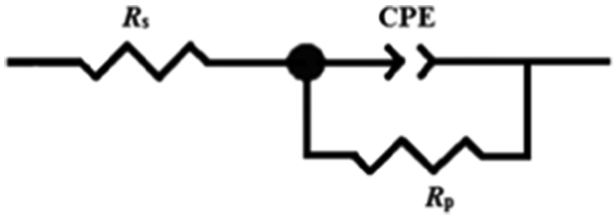

Figure 6. Equivalent circuit model used to analyze the EIS data.

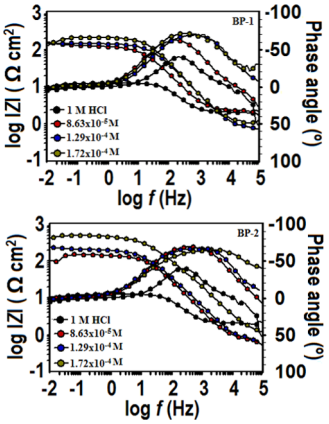

Figure 7. Bode ($\log f$ vs $\log|Z|$) and phase angle ($\log f$ vs $\alpha°$) plots for MS in 1 M HCl without and with bispyrano[2,3-*c*]pyrazoles.

addition of BPs is higher as compared to that in 1 M HCl without BPs. In general, the diameter of the Nyquist arcs is associated with the polarization resistance (R_p).[15−17] The R_p for BPs increases with an increase in concentration, and the highest R_p values for BP-2 and BP-1 are 481.9 and 210.0 Ω cm^2 at 1.72 × 10^{-4} M, respectively.

The inhibition efficiency (η%) was estimated as

$$\eta\% = \left(\frac{R_{p(i)} - R_p}{R_{p(i)}}\right) \times 100 \quad (3)$$

where $R_{p(i)}$ and R_p represent the polarization resistance in the presence and absence of BP-1 and BP-2. The observations from Table 3 reveal that addition of different concentrations of BPs causes an increase in the inhibition efficiency and that for BPs the inhibition order is BP-2 (97.80%) > BP-1 (94.96%) at 1.72 × 10^{-4} M. Moreover, C_{dl} values decrease with increasing BP concentrations. This decreasing C_{dl} points toward/suggests more adsorption of BP molecules on the metal surface, which provide better surface coverage, thereby decreasing the exposed area.[18]

The double layer capacitance (C_{dl}) can be calculated by including CPE parameter values like $Y°$ and n by the equation

$$C_{dl} = \frac{Y°\omega^{n-1}}{\sin(n(\pi/2))} \quad (4)$$

where $Y°$ indicates the CPE constant and n and ω represent the CPE exponent and angular frequency, respectively.

Figure 7 displays the EIS results in Bode resistance and phase angle formats. In general, the ideal capacitive behavior can be recognized when a slope value reaches −1 with phase angle −90°. The deviation of the phase angle along with slope values with BP molecules ranged from 0.71−0.83 to 62−71° compared with the blank slope i.e., −0.54 and phase angle −39°. The movement away/deviation of Bode resistance and phase angle parameter from perfect values confirms the capacitive behavior of MS on addition of BPs.[19]

Polarization plots for MS samples in 1 M HCl without and with different concentrations of BPs are presented in Figure 8.

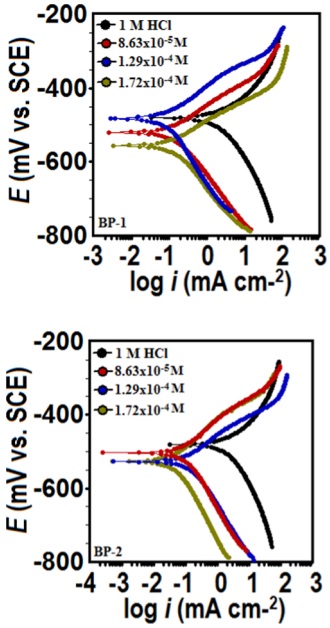

Figure 8. Polarization curves for MS in 1 M HCl without and with bispyrano[2,3-*c*]pyrazoles.

Generally, a potentiodynamic polarization study provides valuable evidence regarding the kinetics involved in the reactions occurring at the anodic and cathodic areas and also what type of inhibition action is taken by corrosion inhibitors on the basis of corrosion potential. It is reported in many research articles that the presence of corrosion inhibitors suppresses the electrochemical reactions (anodic and cathodic) occurring on the metal surface, which results in lowering of the

Table 3. Electrochemical Impedance Parameters for MS in the Absence and Presence of Bispyrano[2,3-*c*]pyrazoles in 1 M HCl

inhibitors	conc. (mol)	R_s(Ω cm^2)	R_p (Ω cm^2)	n	$Y°$	C_{dl} (μF/cm^2)	η%
blank	0.0	2.08	10.58 (0.01)	0.88	294	142	
BP-1	8.63 × 10^{-5}	2.12	123.4 (0.02)	0.85	176	91	91.42
	1.29 × 10^{-4}	0.73	141.8 (0.01)	0.85	126	62	92.53
	1.72 × 10^{-4}	0.93	210.0 (0.02)	0.86	77	40	94.96
BP-2	8.63 × 10^{-5}	0.64	144.3 (0.02)	0.85	137	71	92.66
	1.29 × 10^{-4}	0.37	206.3 (0.01)	0.79	140	59	94.87
	1.72 × 10^{-4}	0.61	481.9 (0.01)	0.74	72	24	97.80

DOI: 10.1021/acsomega.8b01300
ACS Omega 2018, 3, 11151−11162

Table 4. Polarization Parameters for MS in the Absence and Presence of Bispyrano[2,3-*c*]pyrazoles in 1 M HCl

inhibitors	conc. (mol)	i_{corr} (μA/cm^2)	E_{corr} (mV/SCE)	β_a (mV/dec)	$-\beta_c$ (mV/dec)	η%
blank	0.0	1800 (0.01)	−481	73	134	
BP-1	8.63×10^{-5}	168 (0.01)	−520	100	152	90.66
	1.29×10^{-4}	146 (0.02)	−556	85	130	91.88
	1.72×10^{-4}	74 (0.01)	−482	67	102	95.88
BP-2	8.63×10^{-5}	138 (0.02)	−503	118	196	92.33
	1.29×10^{-4}	64.4 (0.01)	−527	55	69	96.42
	1.72×10^{-4}	31.6 (0.01)	−526	67	102	98.24

corrosion current i_{corr}. The decrease in i_{corr} suggested the corrosion inhibition phenomenon.[20,21]

Table 4 presents the values extracted from Tafel fit analysis such as corrosion current density (i_{corr}), corrosion potential (E_{corr}), and cathodic (β_c) and anodic (β_a) Tafel constants. From the obtained results, it is clearly visible that the addition of BPs transfers the corrosion potential toward the more negative direction, which is less than 85 mV compared to that without the inhibitor, signifying a mixed type of inhibitor.[22−24] The β_c and β_a values concurrently changed in a similar pattern on increasing BP concentrations, supporting the mixed action of inhibition.[12] However, for the potential higher than −340 mV/SCE, the presence of BP-2 and BP-2 does not change the current-vs-potential characteristic in the anodic region (Figure 8). This potential can be defined as a desorption potential. Similar results have been reported by some other authors.[25−27] On continuous discussion of results, it is also seen that the addition of BP-1 and BP-2 into 1 M HCl causes a decrease of i_{corr} values (74.0 and 31.6 μA/cm^2 at 1.72×10^{-4} M). The reduction of i_{corr} in the presence of BPs in comparison to that without the inhibitor, i.e., in 1 M HCl (1800 μA/cm^2) for MS, clearly indicated retardation in the electrochemical reaction, resulting in corrosion prevention.

The corrosion inhibition efficiency is calculated by the following equation

$$\eta\% = \frac{i_{corr} - i_{corr}^{\circ}}{i_{corr}} \times 100 \quad (5)$$

where i_{corr}° and i_{corr} are the corrosion current density without and with BP-1 and BP-2, respectively.

2.3. Surface Characterization after Immersion. The surface morphological observation for the steel samples in the test acid solution without and with 1.72×10^{-4} M BP additives, after an exposure period of 6 h at 308 K was carried out by scanning electron microscopy (SEM). The polished MS surface is shown in Figure 9a. The MS samples exposed to 1 M HCl solution are subjected to severe corrosion shown in Figure 9b. On the other hand, a smooth surface with less damages was observed in the case of the MS surface with the addition of BP-1 and BP-2 (Figure 9c,d), which suggests that the MS surface was adequately protected from corrosion by the addition of BPs.[28,29]

Figure 10a−c displays the surface topographic images of the MS surface immersed without and with BP-1 and BP-2 in acid solution. The MS samples immersed in 1 M HCl showed a very rough surface with 188 nm surface roughness, whereas a reduction in surface roughness (48, 24 nm) is obtained in the presence of BP-1 and BP-2, suggesting corrosion inhibition.[30,31]

The IR spectra of pure BP-1 and attenuated total reflection (ATR)-IR study of adsorbed BP-1 on the MS surface are displayed in Figure 11. The observed peaks at 3230, 3104, and 2187 cm^{-1} represent N−H and C≡N stretching peaks for BP-1. From the inspection of ATR-IR spectra (Figure 10) of the inhibited MS, it could be evidently indicated that the observed C≡N and N−H stretching peaks shifted toward lower frequency. This lower frequency shift is attributed to the interaction of BP-1 with MS. In addition with that the mentioned peaks shifted in adsorbed inhibitor spectra of MS surface compared to pure BP-1 suggested the adsorption of inhibitor molecules on steel surface and shift towards lower frequency is attributed owing to the exchange of electrons between metal d orbitals and inhibitor molecules.[32,33]

Figure 12 shows the contact angle images of the MS sample surface in the test acid solution and the inhibited surface by the adsorption of BP-2. The contact angles obtained in the case of MS immersed in blank and inhibited solutions are found to be 74 and 123°, respectively. The lower value of contact angle, 74°, in corroded MS due to direct contact with acid (Figure 12a) shows the hydrophilic nature of corrosion products, which allows water droplets to spread on the MS surface. However, opposite to that, the inhibited MS surface shows a 123° contact angle with the MS surface, representing development of hydrophobic nature after adsorption of inhibitor and supporting corrosion[34] inhibition in the presence of BP-2 (Figure 12b).

The interaction between the BP molecules and MS surface was further examined with X-ray photoelectron spectroscopy (XPS) analysis. Figure 13a displays the low-resolution survey XPS spectra of the blank and inhibited MS surface, and the elements including Fe, C, N, and O were noticed in the case of inhibited MS surface. Figure 13b−e presents the high-resolution deconvoluted profiles for C 1s, N 1s, O 1s, and Fe 2p for the MS surface with the BP-2 inhibitor film. The deconvoluted C 1s spectrum (Figure 13b) for inhibited steel exhibits three key peaks, which indicated the three different chemical states of carbon on the MS surface. The largest peak appearing at 284.65 eV could be ascribed to the C−C, C═C, and C−H aromatic bonds, and the next peak is ascribed to the C−N and C═N bonds in the pyrazole ring with distinctive binding energy (BE) of 283.53 eV. Furthermore, the third peak around 282.62 eV is probably ascribed to the carbon atom of C═N$^+$ in the pyrazole due to the protonation of the ═N− structure in the pyrazole ring and/or the coordination of nitrogen in the pyrazole ring with the MS surface. The XPS spectrum of N 1s (Figure 13c) is decomposed to three components. The first component appearing at 398.52 eV is attributed to the N atom of C−N bonds and the unprotonated N atoms (═N−) in the pyrazole ring. The next component takes the highest influence and might be attributed to coordinate N atoms of pyrazole rings with the MS surface (N−Fe), which shifts toward higher BE. Furthermore, the final component appearing at 400.83 eV may be associated with protonated nitrogen atoms in pyrazole rings. Hence, the

DOI: 10.1021/acsomega.8b01300
ACS Omega 2018, 3, 11151−11162

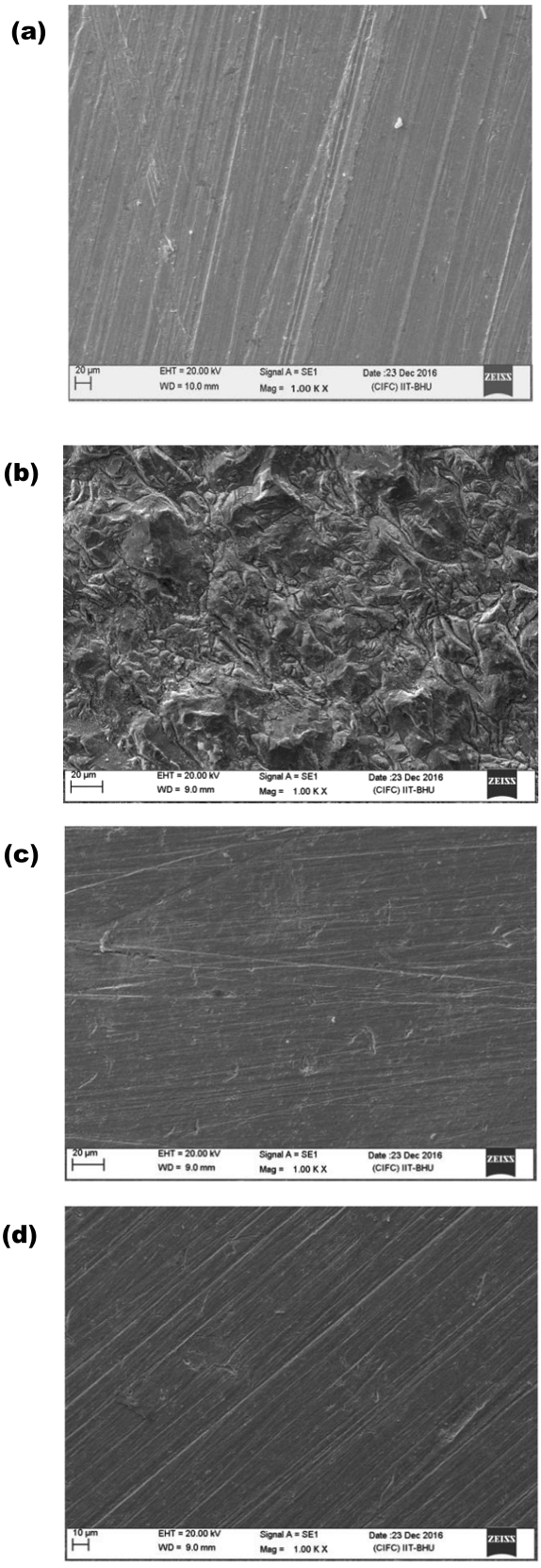

Figure 9. SEM micrographs of (a) polished mild steel, (b) in 1 M HCl, and in the presence of (c) BP-1 and (d) BP-2, at 1.72×10^{-4} M.

appearance of the N 1s peak at 399.96 eV (Figure 13a) specifies the existence of thin layer of BP molecules over the MS surface, and further deconvolution of N 1s signals corroborates the interaction of N atom with the iron surface (N−Fe).[35] Furthermore, the O 1s spectrum at 530.40 eV (Figure 13d) might be ascribed to the production of oxide (Fe_2O_3) on the MS surface.[36−38] The Fe 2p spectrum of MS surface in the presence of BP-2 is displayed in Figure 13e. The Fe 2p spectrum of the MS surface with BP-2 illustrates the double peak profile positioned at around 711.43 eV (Fe $2p_{1/2}$) and 725.32 eV (Fe $2p_{3/2}$), displaying a certain degree of oxidation of the steel surface. From the obtained XPS results, it was supported that chemisorption of BP-2 molecules on the MS surface takes place via sharing of electrons among nitrogen atoms and/or the π electrons and vacant d-orbitals of Fe.

2.4. Quantum Chemical Studies. The quantum chemical calculations are very helpful in attaining more information on the phenomenon of inhibition. The corrosion inhibition performance of an inhibitor is associated with the calculated quantum chemical factors such as E_{HOMO}, E_{LUMO}, ΔE, η, σ, χ, and ΔN and Mulliken charges on the atoms. These parameters can be observed by the optimization of the studied inhibitor molecules.[39,40] These parameters help predict metal−inhibitor interactions. In the present study, all of the quantum parameters were calculated for both neutral and protonated BP molecules in gas phase. The results obtained are summarized in Table 5.

The optimized geometries of neutral and protonated BP-1 and BP-2 are shown in Figures 14 and 15. The inhibitor reactivity can be realized by their frontier molecular orbital energies, E_{HOMO} and E_{LUMO}. The distributions of the frontier molecule orbital density for BPs are presented in Figures 14 and 15. In general, the E_{HOMO} energy value demonstrates the electron donating capacity of the inhibitor. The high value of E_{HOMO} infers that the inhibitor has a high affinity to offer electrons to suitable acceptor molecules, whereas the E_{LUMO} values indicate the electron accepting capacity from metal to inhibitor. Generally, the lower value of E_{LUMO} reveals that the inhibitor can certainly accept electrons from the metal by back-donation. The lower value of ΔE ($\Delta E = E_{LUMO} - E_{HOMO}$) represents good inhibition performance of the molecule.[41,42] The global hardness (GH) and global softness (GS) are other important factors that give information about molecular stability and their reactivity.[43] The energy gap for a hard molecule is large, whereas for a soft molecule, it is low. Hence, the high value of GS and low value of GH suggest a higher corrosion inhibition efficiency.[44,45]

In neutral inhibitor molecules (Figure 14), Table 5 shows that the ΔE value for BP-1 (1.675 eV) is greater than that for BP-2 (1.583 eV), which are very well correlated with the experimental results. The values of global softness (σ) and fraction of electrons transferred (ΔN) for BP-2 > BP-1 and global hardness (η) for BP-2 < BP-1 are also in support of experimental results. The E_{HOMO} value of BP-2 (−3.162 eV) is lower than the E_{HOMO} value of BP-1 (−3.108 eV), which is slightly inconsistent with the experimental results.

The Mulliken charge analysis is useful to estimate the adsorption centers of inhibitors. The more negatively charged the heteroatom, the more the ability to be adsorbed on the metal surface.[22] For BPs, the higher negative charges are found around the nitrogen, oxygen, and some carbon atoms, which indicates that these are the coordinating sites of the inhibitors, but the nitrogen attached as $-NH_2$ with the ring shows that higher negative Mulliken charges have been selected for the protonation sites. The Mulliken charges are given in Table 6.

DOI: 10.1021/acsomega.8b01300
ACS Omega 2018, 3, 11151−11162

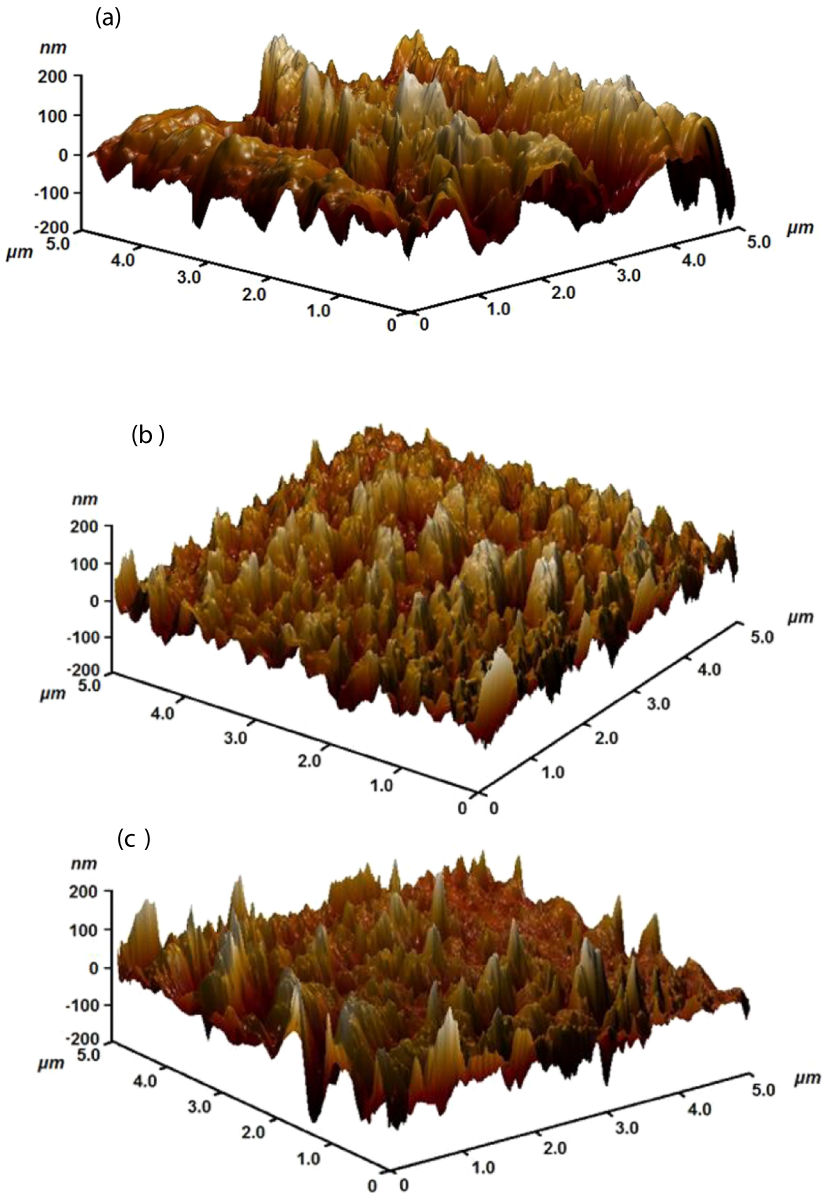

Figure 10. Atomic force microscopy (AFM) micrographs of MS surface in (a) 1 M HCl and in the presence of (b) BP-1 and (c) BP-2, at 1.72 × 10^{-4} M.

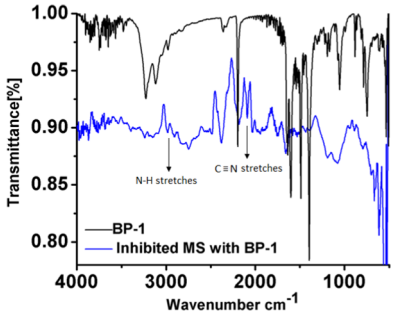

Figure 11. Fourier-transform infrared (FTIR)-ATR spectra of pure BP-1 and inhibited MS.

In the case of protonated inhibitor molecules (Figure 15), the obtained ΔE value for BP-2 (2.140 eV) is lesser than that of BP-1 (2.333 eV), which supports the experimental observations. The discussed parameters like σ, ΔN, and η for neutral molecules show the same supporting experimental trend in the case of protonated molecules, i.e., BP-2 > BP-1 for σ and ΔN and BP-2 < BP-1 for η. The E_{HOMO} value of BP-2 (−7.233 eV) is higher than E_{HOMO} of BP-1 (−7.480 eV), supported very well the experimental results. These findings clearly suggest that BP-2 forms strong bonds with the Fe metal as it shows better inhibition efficiency (98.01%) than that of BP-1 (96.02%).

In the case of protonated inhibitor molecules (Figure 15), the values of E_{HOMO} for BP-1 and BP-2 are lower, −7.480 and −7.233 eV, as compared to those for the neutral molecules (−3.108 and −3.162 eV) due to protonation. It means that the electron donating ability of E_{HOMO} decreases. Therefore, the formation of bond between the inhibitor and the metal occurs by sharing of electrons from the metal to the inhibitor (back-donation). The values of ΔE, ΔN, η, and σ support that BP-2 is a better inhibitor than BP-1. The quantum chemical parameters (ΔE, η, σ, and ΔN) showed good agreement

DOI: 10.1021/acsomega.8b01300
ACS Omega 2018, 3, 11151−11162

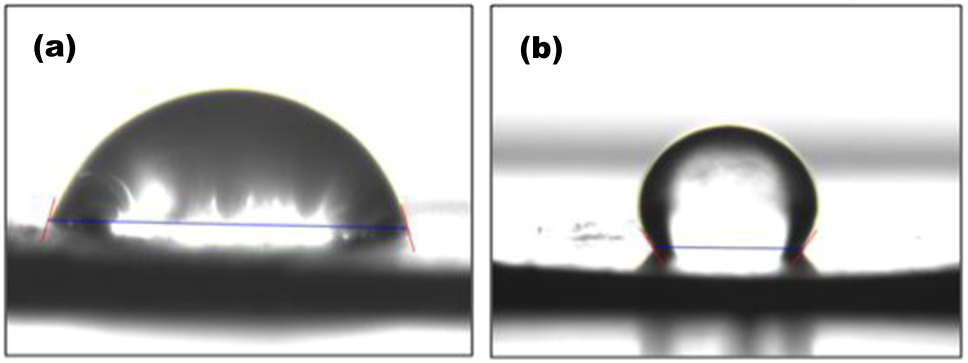

Figure 12. Contact angle measurement pictures for MS exposed to (a) 1 M HCl and (b) 1 M HCl + BP-2.

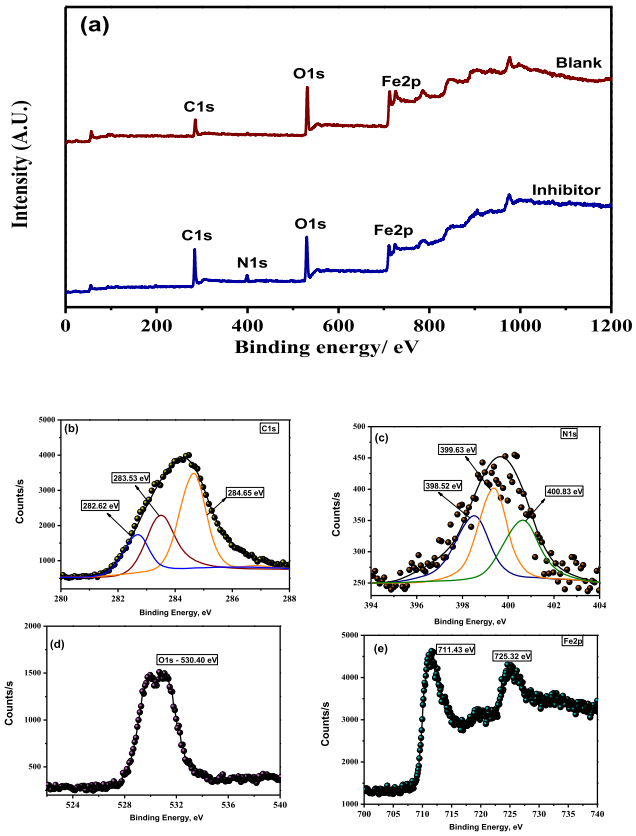

Figure 13. XPS results: (a) survey scan, (b) N 1s, (c) C 1s, (d) O 1s, and (e) Fe 2p for blank and inhibited MS substrates.

Table 5. Calculated Quantum Chemical Parameters for BPs Using DFT-B3LYP/6-31G

compounds → parameters↓	neutral phase		protonated phase	
6-31G	BP-1	BP-2	BP-1	BP-2
E_{HOMO} (eV)	−3.108	−3.162	−7.480	−7.233
E_{LUMO} (eV)	−1.433	−1.579	−5.147	−5.093
ΔE (eV)	1.675	1.583	2.333	2.140
η	0.837	0.791	1.166	1.070
σ	1.194	1.264	0.857	0.934
χ (eV)	2.27	2.37	6.31	6.16
ΔN	1.52	1.54	−0.638	−0.626

with the obtained experimental results, suggesting higher corrosion inhibition efficiency of BP-2 than that of BP-1.

3. CONCLUSIONS

Both the synthesized bispyranopyrazoles BP-1 and BP-2 showed excellent inhibition efficiency of 96.02 and 98.01% at 1.72×10^{-4} M, respectively. BP-2 having a phenyl substituent showed a higher inhibition efficiency than BP-1. EIS analysis showed that an increase in the concentration of inhibitors increases R_p on the metal surface and decreases C_{dl}. Potentiodynamic polarization suggests that the investigated BP-1 and BP-2 acted as mixed-type inhibitors. SEM, AFM, FTIR-ATR, and contact angle studies corroborated the formed inhibitor film on the MS surface. Specifically, XPS studies confirmed the presence of a thin film of inhibitor on the MS surface, which is formed by BP-2 inhibitor molecules via mutual sharing of electrons. The quantum chemical values and experimental results were observed to be in very good agreement.

4. EXPERIMENTAL SECTION

4.1. Materials and Methods. The steel samples (25 mm × 20 mm × 0.6 mm and 80 mm × 10 mm × 0.6 mm) were utilized as base substrates for the gravimetric and electrochemical corrosion tests and have following elemental configuration: Mn-0.596%, Si-0.066%, C-0.066%, P-0.028%, S-0.010%, and remaining iron (wt %). Before each experiment, the MS samples were ground using SiC sheets ranging from 600 to 1200 grade, cleaned with water followed by acetone, and dried. The diluted test solution (1 M HCl) with double-distilled water was prepared using analytical-grade 37% HCl.

4.2. Inhibitors. The two bispyranopyrazoles, 4,4′-(1,4-phenylene)bis(6-amino-3-methyl-2,4-dihydropyrano[2,3-*c*]-pyrazole-5-carbonitrile) (BP-1) and 4,4′-(1,4-phenylene)bis(6-amino-3-methyl-1-phenyl-1,4-dihydropyrano[2,3-*c*]pyrazole-5-carbonitrile) (BP-2), were prepared on the basis of the previous report.[2] Figure 1 shows the schematic route for the synthesis. At the completion of the synthesis, the obtained compound was sieved and rinsed appropriately using EtOH for the desired product. The molecular structures of BP-1 and BP-2 are shown in Table 1. The ^{1}H NMR spectra was recorded using a Bruker instrument at 500 MHz and IR spectra with an FTIR (02) (Perkin Elmer, Bruker) spectrophotometer. The spectral data for BP-1: ^{1}H NMR (500 MHz, DMSO-d_6) δ: d = 1.74 (s, 6H, $2CH_3$), 4.53 (s, 2H, 2CH), 6.79 (s, 4H, $2NH_2$), 7.11 (s, 4H, C_6H_4), 12.07 (s, 2H, 2NH) ppm, IR (KBr) cm^{-1}: 3230, 3104, 2187, 1640, 1585, 1487.

4.3. Gravimetric Measurements. The gravimetric measurements were performed using MS samples in 1 M HCl without and with BP-1 and BP-2. The MS samples were

DOI: 10.1021/acsomega.8b01300
ACS Omega 2018, 3, 11151−11162

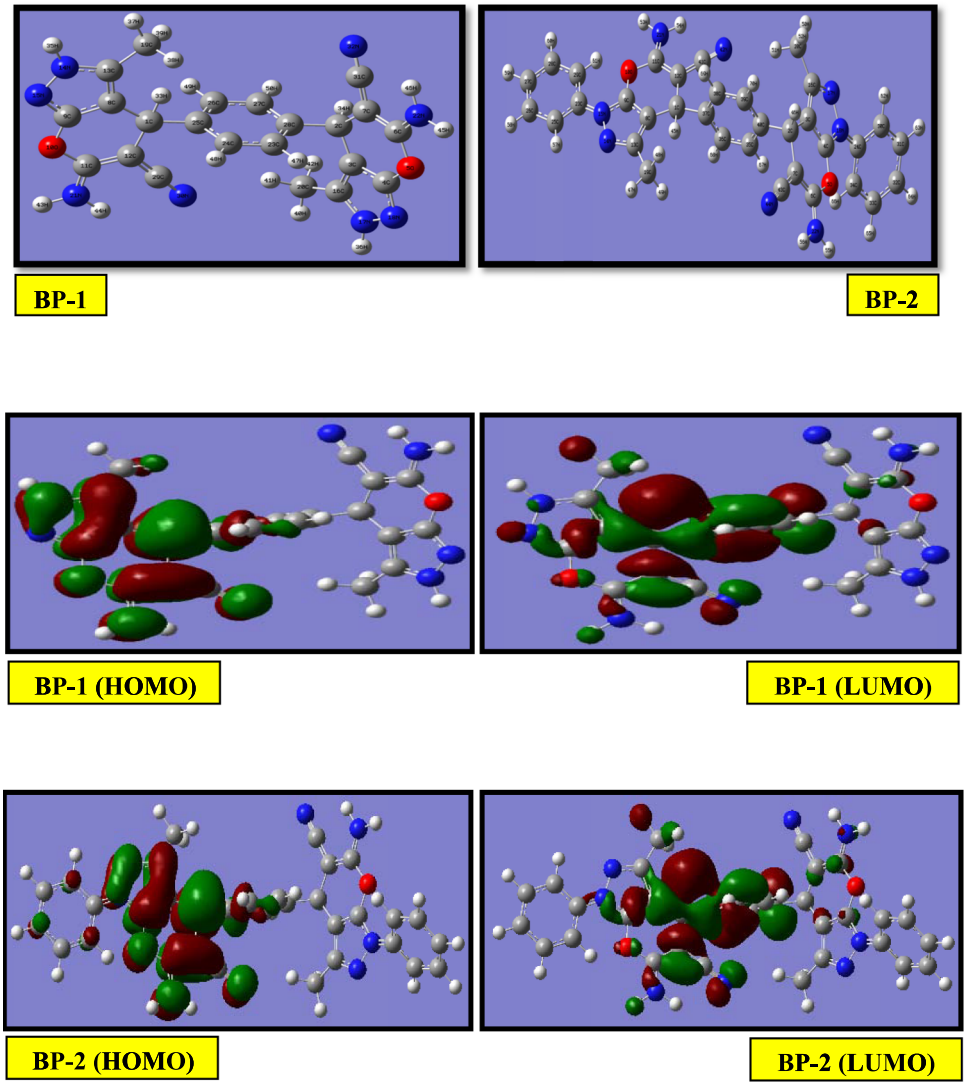

Figure 14. Gas-phase optimized molecular structures and the HOMO and LUMO electron density distribution surfaces of neutral BP-1 and BP-2 molecules.

first ground, washed, dried, and weighted. These specimens were immersed in a 100 mL conical flask for 6 h at 308 K with and without BPs. After the designated exposure period, the MS samples were removed, cleaned with distilled water and subsequently with ethanol, and allowed to dry. The loss in weight was estimated by the difference in weight of MS samples before and after the exposure. The other parameters like corrosion rate (C_R), corrosion inhibition efficiency ($\eta\%$), and MS surface coverage (θ) were calculated by the following equations

$$C_R = \frac{W}{At} \tag{6}$$

$$\eta\% = \frac{C_R - C_{R(i)}}{C_R} \times 100 \tag{7}$$

$$\theta = \frac{C_R - C_{R(i)}}{C_R} \tag{8}$$

where W represents the loss in weight of the specimen (mg), A is the coupon area (cm^2), t is the exposure time (h), and C_R and $C_{R(i)}$ represent the corrosion rates without and with BPs.

4.4. Electrochemical Measurements. Electrochemical corrosion analysis was done by a Gamry G300-45050 potentiostat/galvanostat through a typical three-electrode cell assembly having MS samples (exposure zone of 10 mm^2) acting as working, saturated calomel electrode (SCE) and Pt (platinum) sheet become reference and auxiliary electrode respectively. All of the electrochemical corrosion tests were carried out after a 30 min immersion period for MS to achieve steady open circuit potential (OCP). The EIS test was accomplished with an alternating current amplitude of 10 mV using a frequency region of 10^5–10^{-2} Hz. Furthermore, the potentiodynamic polarization test was performed by adjusting the potential of ±250 mV vs OCP with the scanning speed of 1.0 mV s^{-1}. For data analyses, fitting, and simulations, Gamry Echem Analyst 5.50 software was used.

4.5. Surface Characterization. To investigate the morphological changes on the MS surface before and after the addition of BPs, scanning electron microscopic (SEM) examination was done by the Ziess Evo 50 XVP instrument model at 1.00k× magnifications. The MS samples were initially immersed without and with 1.72×10^{-4} M BP-1 and BP-2 for 6 h at 308 K. After the exposure period, the MS samples were

DOI: 10.1021/acsomega.8b01300
ACS Omega 2018, 3, 11151−11162

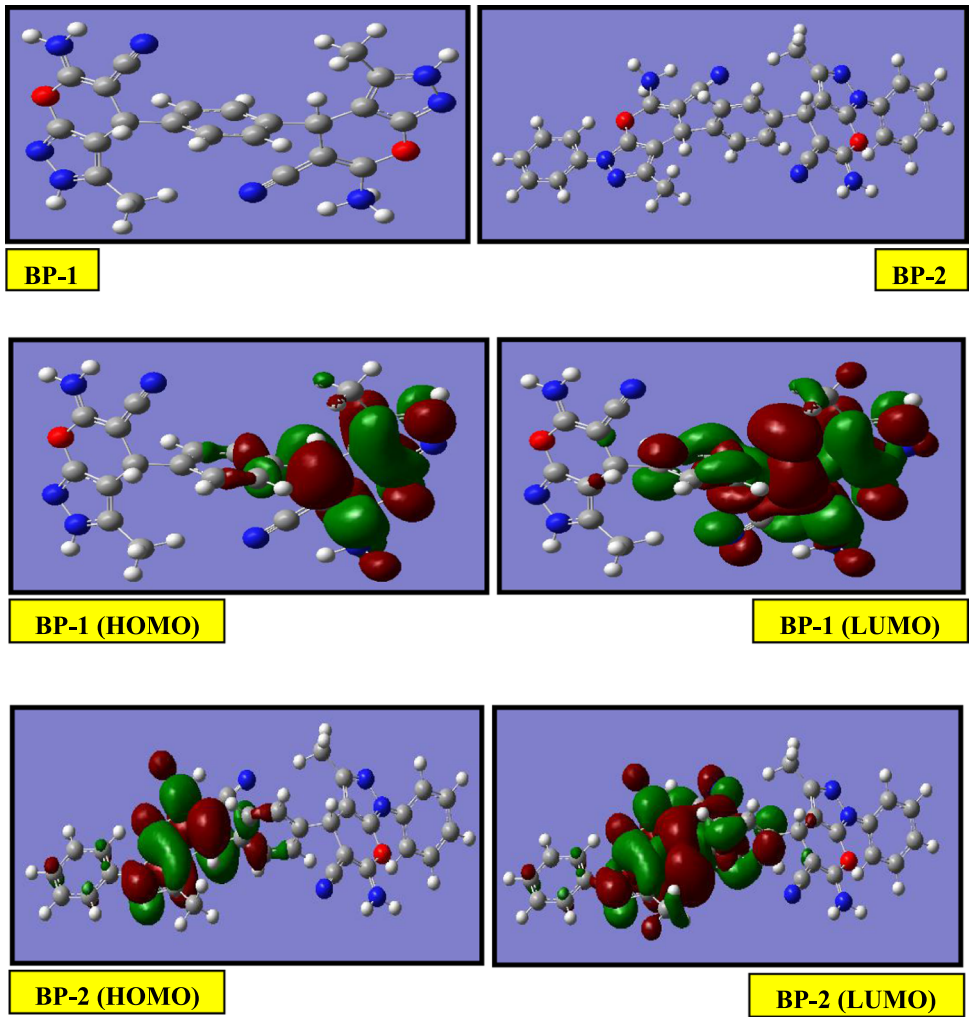

Figure 15. Gas-phase optimized molecular structures and the HOMO and LUMO electron density distribution surfaces of protonated BP-1 and BP-2 molecules.

Table 6. Mulliken Charges of Heteroatoms Present in BPs

	Mulliken charges of heteroatoms									
inhibitors	N_{14}	N_{15}	N_{17}	N_{18}	N_{21}	N_{22}	N_{30}	N_{32}	O_5	O_{10}
BP-1	−0.308	−0.220	−0.295	−0.230	−0.481	−0.475	−0.295	−0.259	−0.308	−0.316
BP-2	−0.289	−0.319	−0.282	−0.304	−0.487	−0.478	−0.281	−0.253	−0.343	−0.409

taken out, rinsed with water followed by ethanol, and allowed to dry to analyze surface microstructure. To investigate the surface topography, AFM was performed by an NT-MDT multimode AFM on the MS sample surface after the exposure period. The attenuated total reflectance study was performed using Bruker-Alpha FTIR spectroscopy with model Eco-ATR. For data analysis, we have used OPUS spectroscopy software. The contact angle study of the MS surface exposed to 1 M HCl without and with BP-2 was executed by Ramé-Hart Goniometer model 250. MS substrates were immersed in 1 M HCl containing 2.0 mM inhibitors for 24 h. After removal from the solutions, the MS samples were washed with ethanol and allowed to dry at room temperature. The X-ray photoelectron spectroscopic (XPS) analysis was done by the Al Kα radiation as a source, and the take-off angle θ was attuned to 45° based on the standard surface.

4.6. Quantum Chemical Studies. Quantum chemical estimations for BP molecules were done in gas phase with both neutral and protonated modes via the DFT approach with the Becke three-parameter hybrid functional along with the Lee–Yang–Paar correlation functional (B3LYP).[46−48] All estimations were done by Gaussian 03 software with the 6-31G(d,p) basis set.[49] The estimated parameters were extracted depending upon the electronic values of the most stable conformers of the investigated inhibitors. The obtained frontier molecular orbital energies such E_{HOMO} and E_{LUMO} help calculate further important factors including ΔE, η, σ, χ, and ΔN using the following equations[50,51]

$$\Delta E = E_{LUMO} - E_{HOMO} \quad (9)$$

$$\eta = -\frac{1}{2}(E_{HOMO} - E_{LUMO}) \quad (10)$$

$$\sigma = \frac{1}{\eta} \quad (11)$$

DOI: 10.1021/acsomega.8b01300
ACS Omega 2018, 3, 11151−11162

$$\chi = -\frac{1}{2}(E_{LUMO} + E_{HOMO}) \quad (12)$$

$$\Delta N = \frac{\chi_{Fe} - \chi_{inh}}{2(\eta_{Fe} + \eta_{inh})} \quad (13)$$

where χ_{Fe} and η_{inh} represent the electronegativity and hardness of Fe, respectively. For χ_{Fe}, a reported magnitude of 7 eV/mol was utilized, whereas for η_{Fe}, 0 eV/mol was used for Fe.[52] Recent literature reveals that the theoretically chosen value of χ_{Fe} = 7 eV is not acceptable because in this case only free electron gas Fermi energy of iron is taken into consideration and electron−electron interaction is neglected. Therefore, to avoid this anomaly, the work function (ϕ) of the metal surface is used in place of χ_{Fe} and the equation is rewritten as

$$\Delta N = \frac{\phi - \chi_{inh}}{2(\eta_{Fe} + \eta_{inh})} \quad (14)$$

For an iron surface having a higher stabilization energy and packed surface, i.e., Fe(110) is used, and its DFT-derived ϕ value is 4.82.[53]

AUTHOR INFORMATION

Corresponding Authors

*E-mail: priyankasingh.rs.apc@itbhu.ac.in (P.S.).
*E-mail: maquraishi.apc@itbhu.ac.in, mumtaz.quraishi@kfupm.edu.sa. Phone: +966538600057 (M.A.Q.).

ORCID

Priyanka Singh: 0000-0002-8947-9796
Mumtaz Ahmad Quraishi: 0000-0002-7822-0084

Notes

The authors declare no competing financial interest.

ACKNOWLEDGMENTS

P.S. is thankful to SERB-National Post-doctoral Fellowship (N-PDF), DST, India, for the financial assistance and University of Delhi for facilitation of this study.

REFERENCES

(1) Vasuki, G.; Kumaravel, K. Rapid four-component reactions in water: synthesis of Pyranopyrazoles. *Tetrahedron Lett.* **2008**, *49*, 5636−5638.

(2) Ablajan, K.; Wang, L. J.; Maimaiti, Z.; Lu, Y. T. CeCl3-promoted one-pot synthesis of multisubstituted bispyrano[2,3-c]pyrazole derivatives. *Monatsh. Chem.* **2014**, *145*, 491−496.

(3) Kumar, S.; Sharma, D.; Yadav, P.; Yadav, M. Experimental and Quantum Chemical Studies on Corrosion Inhibition Effect of Synthesized Organic Compounds on N80 Steel in Hydrochloric Acid. *Ind. Eng. Chem. Res.* **2013**, *52*, 14019−14029.

(4) Singh, P.; Singh, A.; Quraishi, M. A. Inhibition effect of 1,3,5-tri-p-tolyl-1,3,5-triazene on the corrosion of brass in 0.5 M HCl solution. *Res. Chem. Intermed.* **2014**, *40*, 595−604.

(5) Sulaiman, K. O.; Onawole, A. T. Quantum chemical evaluation of the corrosion inhibition of novel aromatic hydrazide derivatives on mild steel in hydrochloric acid. *Comput. Theor. Chem.* **2016**, *1093*, 73−80.

(6) Turcio-Ortega, D.; Pandiyan, T.; Cruz, J.; Garcia-Ochoa, E. Interaction of Imidazoline Compounds with Fen (n) 1-4 Atoms) as a Model for Corrosion Inhibition: DFT and Electrochemical Studies. *J. Phys. Chem. C* **2007**, *111*, 9853−9866.

(7) Yadav, D. K.; Quraishi, M. A. Electrochemical investigation of Substituted Pyranopyrazoles Adsorption on Mild Steel in Acid Solution. *Ind. Eng. Chem. Res.* **2012**, *51*, 8194−8210.

(8) Gupta, N. K.; Verma, C.; Salghi, R.; Lgaz, H.; Mukherjee, A. K.; Quraishi, M. A. New phosphonate based corrosion inhibitors for mild steel in hydrochloric acid useful for industrial pickling processes: experimental and theoretical approach. *New J. Chem.* **2017**, *41*, 13114−13129.

(9) Wang, C.; Lai, C.; Xie, B.; Guo, X.; Fu, D.; Li, B.; Zhu, S. Corrosion Inhibition of Mild Steel in HCl Medium by S-benzyl-O,O′-bis(2-naphthyl)dithiophosphate with Ultra-long Lifespan. *Results Phys.* **2018**, *10*, 558−567.

(10) Haque, J.; Verma, C.; Srivastava, V.; Quraishi, M. A.; Ebenso, E. E. Experimental and quantum chemical studies of functionalized tetrahydropyridines as corrosion inhibitors for mild steel in 1 M hydrochloric acid. *Results Phys.* **2018**, *9*, 1481−1493.

(11) Verma, C.; Olasunkanmia, L. O.; Ebensoa, E. E.; Quraishi, M. A. Substituents effect on corrosion inhibition performance of organic compounds in aggressive ionic solutions: A review. *J. Mol. Liq.* **2018**, *251*, 100−118.

(12) Singh, P.; Ebenso, E. E.; Olasunkanmi, L. O.; Obot, I. B.; Quraishi, M. A. Electrochemical, Theoretical, and Surface Morphological Studies of Corrosion Inhibition Effect of Green Naphthyridine Derivatives on Mild Steel in Hydrochloric Acid. *J. Phys. Chem. C* **2016**, *120*, 3408−3419.

(13) Mishra, A.; Verma, C.; Lgaz, H.; Srivastava, V.; Quraishi, M. A.; Ebenso, E. E. Synthesis, characterization and corrosion inhibition studies of N-phenyl-benzamides on the acidic corrosion of mild steel: Experimental and computational studies. *J. Mol. Liq.* **2018**, *251*, 317−332.

(14) Solmaz, R. Investigation of Adsorption and Corrosion Inhibition of Mild Steel in Hydrochloric Acid Solution by 5-(4-Dimethylaminobenzylidene)Rhodanine. *Corros. Sci.* **2014**, *79*, 169−176.

(15) Haldhar, R.; Prasad, D.; Saxena, A.; Singh, P. Valeriana wallichii root extract as a green & sustainable corrosion inhibitor for mild steel in acidic environments: experimental and theoretical study. *Mater. Chem. Front.* **2018**, *2*, 1225−1237.

(16) Solmaz, R. Investigation of the Inhibition Effect of 5-((E)-4-phenylbuta-1,3-dienylideneamino)-1,3,4-thiadiazole-2-thiol Schiff Base on Mild Steel Corrosion in Hydrochloric Acid. *Corros. Sci.* **2010**, *52*, 3321−3330.

(17) Saha, S. K.; Dutta, A.; Ghosh, P.; Sukul, D.; Banerjee, P. Novel Schiff-base molecules as efficient corrosion inhibitors for mild steel surface in 1 M HCl medium: experimental and theoretical approach. *Phys. Chem. Chem. Phys.* **2016**, *18*, 17898−17911.

(18) Ansari, K. R.; Quraishi, M. A.; Singh, A. Corrosion Inhibition of Mild Steel in Hydrochloric Acid by some Pyridine Derivatives: An Experimental and Quantum Chemical Study. *J. Ind. Eng. Chem.* **2015**, *25*, 89−98.

(19) Dandia, A.; Gupta, S. L.; Singh, P.; Quraishi, M. A. Ultrasound-Assisted Synthesis of Pyrazolo[3,4-*b*]pyridines as Potential Corrosion Inhibitors for Mild Steel in 1.0 M HCl. *ACS Sustainable Chem. Eng.* **2013**, *1*, 1303−1310.

(20) Srivastava, V.; Haque, J.; Verma, C.; Singh, P.; Lgaz, H.; Salghi, R.; Quraishi, M. A. Amino acid based imidazolium zwitterions as novel and green corrosion inhibitors for mild steel: Experimental, DFT and MD studies. *J. Mol. Liq.* **2017**, *244*, 340−352.

(21) Saxena, A.; Prasad, D.; Haldhar, R.; Singh, G.; Kumar, A. Use of *Sida cordifolia* extract as green corrosion inhibitor for mild steel in 0.5 M H2SO. *J. Environ. Chem. Eng.* **2018**, *6*, 694−700.

(22) Umoren, S. A.; Obot, I. B.; Israel, A. U.; Asuquo, P. O.; Solomon, M. M.; Eduok, U. M.; Udoh, A. P. Inhibition of Mild Steel Corrosion in Acidic Medium using Coconut Coir Dust Extracted from Water and Methanol as Solvents. *J. Ind. Eng. Chem.* **2014**, *20*, 3612−3622.

(23) Kosari, A.; Moayed, M. H.; Davoodi, A.; Parvizi, R.; Momeni, M.; Eshghi, H.; Moradi, H. Electrochemical and Quantum Chemical Assessment of Two Organic Compounds from Pyridine Derivatives as Corrosion Inhibitors for Mild Steel in HCl Solution Under Stagnant Condition and Hydrodynamic Flow. *Corros. Sci.* **2014**, *78*, 138−150.

DOI: 10.1021/acsomega.8b01300
ACS Omega 2018, 3, 11151−11162

(24) Yadav, D. K.; Quraishi, M. A. Application of Some Condensed Uracils as Corrosion Inhibitors for Mild Steel: Gravimetric, Electrochemical, Surface Morphological, UV−Visible, and Theoretical Investigations. *Ind. Eng. Chem. Res.* **2012**, *51*, 14966−14979.
(25) Zarrouk, A.; Hammouti, B.; Lakhlifi, T.; Traisnel, M.; Vezin, H.; Bentiss, F. New 1H-pyrrole-2,5-dione derivatives as efficient organic inhibitors of carbon steel corrosion in hydrochloric acid medium: Electrochemical, XPS and DFT studies. *Corros. Sci.* **2015**, *90*, 572−584.
(26) Bentiss, F.; Traisnel, M.; Gengembre, L.; Lagrene, M. A new triazole derivative as inhibitor of the acid corrosion of mild steel: electrochemical studies, weight loss determination, SEM and XPS. *Appl. Surf. Sci.* **1999**, *152*, 237−249.
(27) Gao, G.; Liang, C. Electrochemical and DFT studies of -amino-alcohols as corrosion inhibitors for brass. *Electrochim. Acta* **2007**, *52*, 4554−4559.
(28) Verma, C.; Olasunkanmi, L. O.; Ebenso, E. E.; Quraishi, M. A.; Obot, I. B. Adsorption Behavior of Glucosamine-Based, Pyrimidine-Fused Heterocycles as Green Corrosion Inhibitors for Mild Steel: Experimental and Theoretical Studies. *J. Phys. Chem. C* **2016**, *120*, 11598−11611.
(29) Singh, P.; Quraishi, M. A. Corrosion inhibition of mild steel using Novel Bis Schiff's Bases as corrosion inhibitors: Electrochemical and Surface measurement. *Measurement* **2016**, *86*, 114−124.
(30) Vashisht, H.; Bahadur, I.; Kumar, S.; Goyal, M. S.; Kaur, G.; Singh, G.; Katata-Seru, L.; Ebenso, E. E. Synergistic interactions between tetra butyl phosphonium hydroxide and iodide ions on the mild steel surface for corrosion inhibition in acidic medium. *J. Mol. Liq.* **2016**, *224*, 19−29.
(31) Singh, P.; Srivastava, V.; Quraishi, M. A. Novel quinoline derivatives as green corrosion inhibitors for mild steel in acidic medium: Electrochemical, SEM, AFM, and XPS studies. *J. Mol. Liq.* **2016**, *216*, 164−173.
(32) Kumar, R.; Yadav, O. S.; Singh, G. Electrochemical and surface characterization of a new eco-friendly corrosion inhibitor for mild steel in acidic media: A cumulative study. *J. Mol. Liq.* **2017**, *237*, 413−427.
(33) Kumar, R.; Chopra, R.; Singh, G. Electrochemical, morphological and theoretical insights of a new environmentally benign organic inhibitor for mild steel corrosion in acidic media. *J. Mol. Liq.* **2017**, *241*, 9−19.
(34) Bandeira, R. M.; Drunen, J.; Garcia, A. C.; Filho, G. T. Influence of the thickness and roughness of polyaniline coatings on corrosion protection of AA7075 aluminum alloy. *Electrochim. Acta* **2017**, *240*, 215−224.
(35) Bentiss, F.; Jama, C.; Mernari, B.; El Attari, H.; El Kadi, L.; Lebrini, M.; Traisnel, M.; Lagrené, M. Corrosion control of mild steel using 3,5-bis(4-methoxyphenyl)-4-amino-1,2,4-triazole in normal hydrochloric acid medium. *Corros. Sci.* **2009**, *51*, 1628−1635.
(36) Zhang, D.; An, Z.; Pan, Q.; Gao, L.; Zhou, G. Comparative study of bis-piperidiniummethyl-urea and mono-piperidiniummethyl-urea as volatile corrosion inhibitors for mild steel. *Corros. Sci.* **2006**, *48*, 1437−1448.
(37) Zhang, Z.; Chen, S.; Li, Y.; Li, S.; Wang, L. A study of the inhibition of iron corrosion by imidazole and its derivatives self-assembled films. *Corros. Sci.* **2009**, *51*, 291−300.
(38) Obot, I. B.; Madhankumar, A.; Umoren, S.; Gasem, Z. Surface protection of mild steel by benzimidazole derivatives: Electrochemical evaluation, weight loss study, surface analyses and theoretical approaches. *J. Adhes. Sci. Technol.* **2015**, *29*, 2130−2152.
(39) Singh, P.; Singh, A.; Quraishi, M. A. Thiopyrimidine derivatives as new and effective corrosion inhibitors for mild steel in hydrochloric acid: Electrochemical and quantum chemical studies. *J. Taiwan Inst. Chem. Eng.* **2016**, *60*, 588−601.
(40) Mendonça, G. L. F.; Costa, S. N.; Freire, V. N.; Casciano, P. N. S.; Correia, A. N.; de Lima-Neto, P. Understanding the corrosion inhibition of carbon steel and copper in sulphuric acid medium by amino acids using electrochemical techniques allied to molecular modelling methods. *Corros. Sci.* **2017**, *115*, 41−55.
(41) Ansari, K. R.; Quraishi, M. A. Experimental and Computational Studies of Naphthyridine Derivatives as Corrosion Inhibitor for N80 Steel in 15% Hydrochloric Acid. *Phys. E* **2015**, *69*, 322−331.
(42) Singh, P.; Makowska-Janusik, M.; Slovensky, P.; Quraishi, M. A. Nicotinonitriles as green corrosion inhibitors for mild steel in hydrochloric acid: Electrochemical, computational and surface morphological studies. *J. Mol. Liq.* **2016**, *220*, 71−81.
(43) Abd El-Lateef, H. M. Experimental and computational investigation on the corrosion inhibition characteristics of mild steel by some novel synthesized imines in hydrochloric acid solutions. *Corros. Sci.* **2015**, *92*, 104−117.
(44) Abd El-Lateef, H. M.; Abu-Dief, A. M.; Abdel-Rahman, L. H.; Sanudo, E. C.; Aliaga-Alcalde, N. Electrochemical and theoretical quantum approaches on the inhibition of C1018 carbon steel corrosion in acidic medium containing chloride using some newly synthesized phenolic Schiff bases compounds. *J. Electroanal. Chem.* **2015**, *743*, 120−133.
(45) Olasunkanmi, L. O.; Obot, I. B.; Ebenso, E. E. Adsorption and corrosion inhibition properties of N-{n-[1-R-5-(quinoxalin-6-yl)-4,5-dihydropyrazol- 3 yl] phenyl} methane sulfon amides on mild steel in 1 M HCl: experimental and theoretical studies. *RSC Adv.* **2016**, *6*, 86782−86797.
(46) Becke, A. D. Density-Functional Thermochemistry. III. The Role of Exact Exchange. *J. Chem. Phys.* **1993**, *98*, 5648−5652.
(47) Becke, A. D. Density-Functional Exchange-energy Approximation with correct Asymptotic Behaviour. *Phys. Rev. A* **1988**, *38*, 3098−3100.
(48) Lee, C.; Yang, W.; Parr, R. G. Development of the Colle-Salvetti Correlation-energy Formula into a Functional of the Electron Density. *Phys. Rev. B* **1988**, *37*, 785−789.
(49) Frisch, M. J.; et al. *Gaussian 03*, revision E.01; Gaussian Inc.: Wallingford, CT, 2007.
(50) Martinez, S. Inhibitory Mechanism of Mimosa Tannin using Molecular Modeling and Substitutional Adsorption Isotherms. *Mater. Chem. Phys.* **2003**, *77*, 97−102.
(51) Olasunkanmi, L. O.; Obot, I. B.; Kabanda, M. M.; Ebenso, E. E. Some Quinoxalin-6-yl Derivatives as Corrosion Inhibitors for Mild Steel in Hydrochloric Acid: Experimental and Theoretical Studies. *J. Phys. Chem. C* **2015**, *119*, 16004−16019.
(52) Pearson, R. G. Absolute Electronegativity and Hardness: Application to Inorganic Chemistry. *Inorg. Chem.* **1988**, *27*, 734−740.
(53) Singh, A.; Ansari, K. R.; Haque, J.; Dohare, P.; Lgaz, H.; Salghi, R.; Quraishi, M. A. Effect of electron donating functional groups on corrosion inhibition of mild steel in hydrochloric acid: Experimental and quantum chemical study. *J. Taiwan Inst. Chem. Eng.* **2018**, *82*, 233−251.

DOI: 10.1021/acsomega.8b01300
ACS Omega 2018, 3, 11151−11162